

Dynamics of Oxidation of Aluminum Nanoclusters using Variable Charge Molecular-Dynamics Simulations on Parallel Computers

Timothy Campbell, Rajiv K. Kalia, Aiichiro Nakano, and Priya Vashishta

Concurrent Computing Laboratory for Materials Simulations, Department of Physics and Astronomy and Department of Computer Science, Louisiana State University, Baton Rouge, Louisiana 70803

Shuji Ogata

Department of Applied Sciences, Yamaguchi University, 2557 Tokiwadai, Ube 755-8611, Japan

Stephen Rodgers

AFRL/PRS, Propulsion Science Division, 10 East Saturn Road, Edwards AFB, California 93524-7680
(Received 18 November 1998)

Oxidation of aluminum nanoclusters is investigated with a parallel molecular-dynamics approach based on dynamic charge transfer among atoms. Structural and dynamic correlations reveal that significant charge transfer gives rise to large negative pressure in the oxide which dominates the positive pressure due to steric forces. As a result, aluminum moves outward and oxygen moves towards the interior of the cluster with the aluminum diffusivity 60% higher than that of oxygen. A stable 40 Å thick amorphous oxide is formed; this is in excellent agreement with experiments. [S0031-9007(99)09416-8]

PACS numbers: 61.46.+w, 81.05.Bx, 81.05.Ys, 81.65.Mq

In recent times, consolidated solids composed of nanometer size clusters (nanophase materials) have drawn a great deal of attention because of their unique thermomechanical, electrical, and magnetic properties [1]. In contrast to conventional polycrystalline solids, nanophase materials have a large fraction of atoms in the interfacial regions, which has a dramatic effect on the structure and physical properties of these materials [2]. A particularly interesting possibility in nanophase materials is the synthesis of nanostructured composites consisting of metallic nanoclusters coated with a passivation layer. Upon compaction, the passivation layer forms a boundary layer between the isolated metallic grains. The presence of the passivating network is known to have a dramatic effect on the electrical, chemical, and mechanical behavior of the material. In a recent study by Sánchez-López *et al.* [3], Al/Al-oxide nanocomposites were found to have a metallic shine and an Ohmic electrical resistivity that was dependent upon the compaction conditions. The nanocomposite consisted of 300 Å aluminum particles with an interconnected 40 Å oxide layer that prevented the material from falling apart when heated to temperatures above the melting point of aluminum. Other studies point out that the properties of these nanocomposite materials are strongly dependent on the nature of the passivation layer [4].

In this Letter we report the first successful molecular-dynamics (MD) simulation of the oxidation of an Al nanocluster (diameter 200 Å). We have investigated the structural and dynamic correlations in the oxide region and the evolution of various quantities including charge, surface oxide thickness, diffusivities of atoms, and local stresses. The MD simulations are based on a highly

reliable interaction scheme developed by Streit and Mintmire [5] that can successfully describe a wide range of physical properties of Al and Al₂O₃. This scheme is capable of treating: (i) both metallic and ceramic systems, (ii) bond formation and bond breakage, and (iii) changes in charge transfer as the atoms move and their local environments are constantly altered. Dynamic charge transfer gives rise to a computationally intensive Coulomb interaction which, for the number of atoms necessary in a realistic simulation, requires highly efficient algorithms that map well onto parallel architectures. We have implemented the fast multipole method of Greengard and Rokhlin [6] for the long-range Coulomb interaction [this reduces the computational complexity from $O(N^2)$ to $O(N)$] with extensions for stress calculations, and the multiple time-step algorithm of Tuckerman *et al.* [7] (this can further reduce the execution time by an order of magnitude). Both algorithms are well suited for parallel architectures.

The setup for the oxidation simulations is as follows. A fcc-crystalline Al sphere (diameter = 200 Å) composed of 252 158 atoms and thermalized at 300 K is placed at the center of a cubic box of length 800 Å. A total of 530 720 oxygen are distributed randomly outside the Al sphere (radius 110 to 400 Å) in the form of molecular (O₂) oxygen at a temperature of 300 K. The oxygen density is 40 times that of the normal state (1 atm and 300 K). A spherical reflecting wall of radius 400 Å confines the entire system. The equations of motion are integrated with time steps $\Delta t = 1$ fs for short-range forces and $\Delta t = 20$ fs for long-range forces. New atomic charges are determined every 100 time steps such that the electrostatic energy is minimized subject to the constraint

that the total system remains neutral. Canonical MD simulation, in which the temperature of the whole system is fixed at 400 K using the Nose-Hoover thermostat chain [8], is performed.

Figure 1 shows the oxide thickness as a function of the simulation time for the first 260 ps. The oxide thickness increases linearly with time during the first 50 ps and subsequently the rate becomes smaller and the thickness saturates at 33 Å. The inset of Fig. 1 is a plot of the inner and outer radial extents of the oxide. The growth of the oxide scale is both inward and outward: inward because of the movement of oxygen towards the interior of the cluster and outward because of the movement of aluminum towards the oxide surface. The inward and outward growth of the oxide saturate at 77 and 110 Å, respectively, with the inward growth saturating later than the outward.

Analysis of local stresses reveal large stress gradients throughout the nanocluster with the oxide largely under negative pressure and the metal core under positive pressure. Local pressures range between -1 and 1 GPa. (The local stresses were calculated by averaging the atomic virial in 6 Å voxels over a 1 ps interval.) The local stress regions are further examined by separating the contributions from the electrostatic and nonelectrostatic forces. Figure 2 depicts the electrostatic and nonelectrostatic force contributions to the local pressure after 100 ps. It can be seen from Fig. 2(a) that the attractive Coulomb force between aluminum and oxygen contributes a large negative pressure localized in the oxide. The electrostatic pressure contribution increases in magnitude toward the middle of the oxide where charge transfer is the highest. The large attractive forces are partially offset by steric repulsion which gives rise to a positive nonelectrostatic contribution to the local pressure in the oxide; see Fig. 2(b).

The large stress gradients give rise to diffusion of atoms in the oxide region. Analysis of the atomic diffusivities in the oxide show that during the first 100 ps

the diffusivity of aluminum is 30% to 60% larger than that of oxygen. (This is due to the smaller steric size of aluminum.) We calculate diffusivities from mean-square displacements computed over a 1 ps interval. At 50 ps the diffusivities of aluminum and oxygen are 1.4×10^{-4} and 1.1×10^{-4} cm²/s, respectively. By 100 ps the diffusivity of oxygen has dropped to 7.4×10^{-5} cm²/s, while that of aluminum decreases to only 1.2×10^{-4} cm²/s. The radial and tangential diffusivities remain about equal, indicating that while the oxide grows radially, high tangential diffusion causes uniformity in the oxide thickness with respect to polar angles.

Saturation of the oxide growth during the first 260 ps is accompanied by a depletion of oxygen outside the nanocluster. In order to bring the oxide as close as possible to complete saturation, we continue the simulation in the canonical ensemble to 466 ps while maintaining the oxygen density, n_0 , outside the nanocluster in the range 0.001 – 0.002 Å⁻³. An oxide scale of 40 Å thickness is subsequently formed, as seen in Fig. 3, which is a snapshot of a small slice (115 Å \times 115 Å \times 8 Å) of the system at 466 ps. The outer radial extent of the oxide remains at 110 Å; however, the inner radial extent moves to 70 Å. The average mass density of the oxide is 2.9 g/cm³ ($n_{\text{Al}} = 0.042$ Å⁻³ and $n_{\text{O}} = 0.038$ Å⁻³), which is about 75% of the crystalline α -Al₂O₃ density. Charge transfer in the oxide is significant and decreases in magnitude near the interfaces; see Fig. 3.

Aluminum nanoclusters of diameters 100 – 700 Å are known to form an oxide scale with thickness between 20 and 50 Å in oxygen gases at room temperature [3,4]. The thickness of oxide scales as a function of cluster size for small metallic clusters have been measured [9]. For Al clusters of diameter 200 Å the thickness is 30 – 40 Å. Remarkable similarity in the oxide thickness is found between the present simulation results and the experimental observations.

In all of the known literature there is no detailed structural analysis of the oxide scale on Al nanoclusters.

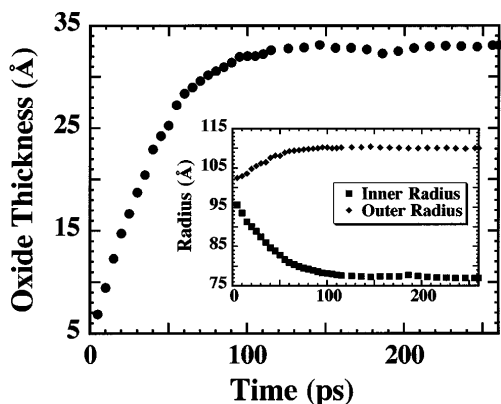


FIG. 1. Thickness of the oxide layer as a function of simulation time. The inner and outer radial extents of the oxide layer as a function of simulation time are shown in the inset.

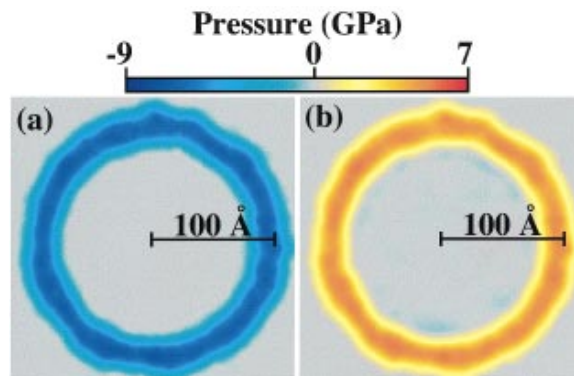


FIG. 2(color). (a) Electrostatic and (b) nonelectrostatic contributions to the local pressure in the nanocluster after 100 ps of simulation time.

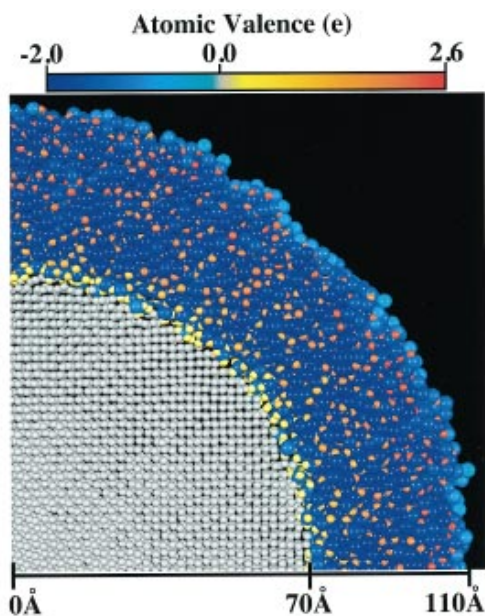


FIG. 3(color). Snapshot of a small slice ($115 \text{ \AA} \times 115 \text{ \AA} \times 8 \text{ \AA}$) of the Al nanocluster after 466 ps of simulation time. The larger spheres correspond to oxygen and smaller spheres to aluminum; color represents the sign and magnitude of the charge on an atom.

Recent studies have pointed out that the local structure of the amorphous oxide scale for Al nanoclusters is different from the amorphous scale that forms on the bulk Al surface [4]. However, details of the differences between the two amorphous oxides are not known.

We analyze structural correlations in the oxide scale through partial pair-distribution functions, coordination numbers, and bond-angle distributions. Figure 4(a) shows the Al-O pair-distribution function for three spherical shells in the oxide scale. These results show a variation of structures as we pass through the oxide from the metal-

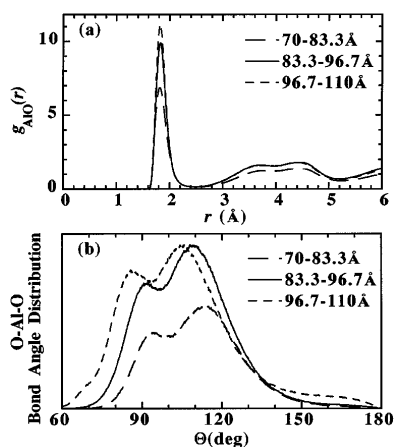


FIG. 4. Structural correlations in three spherical shells of the oxide scale: (a) Al-O pair-distribution functions; (b) O-Al-O bond-angle distributions.

oxide interface (70–83.3 Å) to the oxide interior (83.3–96.7 Å) and on to the oxide-environment interface (96.7–110 Å). In Fig. 4(a) we observe that the position of the first peak in $g_{AlO}(r)$ gives the Al-O bond length to be around 1.81 Å in the metal-oxide interface. The Al-O peak shifts slightly toward larger r in the interior and oxide-environmental regions. Pair-distribution functions for Al-Al and O-O also show shifts in the peak positions related to the change in the relative Al and O densities in each region. The corresponding coordination numbers for Al in each region [obtained by integrating $g_{AlO}(r)$ up to 2.5 Å] are 3.1 for the metal-oxide interface, 3.9 in the interior of the oxide region, and 4.3 for the oxide-environment interface.

Figure 4(b) shows the O-Al-O bond-angle distribution for each region in the oxide scale. We see that throughout the oxide there are two distinct peaks in the bond-angle distribution. In the interior of the oxide the distribution shows peaks at 90° and 109°. These peaks shift toward smaller angles in the oxide-environment interface, reflecting the decrease in aluminum density. In the metal-oxide interface where the oxygen density is lower, we observe that the peaks in the bond-angle distribution shift toward larger angles. The two peaks in the oxide region indicate mixed octahedral, $Al(O_{1/6})_6$, and tetrahedral, $Al(O_{1/4})_4$, configurations.

It is interesting to compare the present results with those for liquid alumina, which is made up of tetrahedrally coordinated aluminum [10], and amorphous alumina formed by anodization, which consists of a mixture of tetrahedrally and octahedrally coordinated aluminum [11,12]. Additionally, aluminum ions in porous alumina films are known to be predominately tetrahedrally (or even lower) coordinated [12]. Reported Al-O bond lengths in amorphous Al_2O_3 films range from 1.8 to 1.9 Å, depending on the porosity and method of preparation [12].

Recent experiments have demonstrated that small aluminum particles are highly explosive under high oxygen pressure and closed conditions [13]. Motivated by this experimental observation, we simulated the oxidation behavior in closed conditions without heat dissipation, i.e., the simulations were performed in the microcanonical ensemble. Figure 5 shows the evolution of oxidation in a small slice ($130 \text{ \AA} \times 130 \text{ \AA} \times 8 \text{ \AA}$) of the microcanonical simulation. Energy released from Al-O bond formation is rapidly transported into the nanocluster resulting in disordering of the Al nanocrystal and outward expansion of the oxide region. The thickness of the oxide region increases linearly with time and does not saturate. By 50 ps the thickness and temperature of the oxide region are 35 Å and 2500 K, respectively. Subsequently, numerous small Al_xO_y fragments are ejected from the nanocluster surface, indicating that the nanocluster is exploding. This behavior under closed conditions has also been observed experimentally [13].

In conclusion, we report the first molecular-dynamics simulation study of the oxidation of aluminum

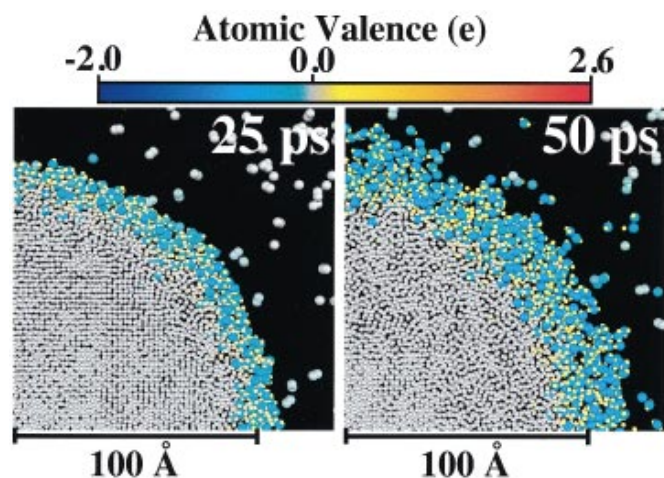


FIG. 5(color). Snapshots showing the evolution of oxidation in a small slice ($130 \text{ \AA} \times 130 \text{ \AA} \times 8 \text{ \AA}$) of the Al nanocluster in the microcanonical ensemble. The larger spheres correspond to oxygen and smaller spheres to aluminum; color represents the sign and magnitude of the charge on an atom.

nanoclusters. The simulations incorporate dynamic charge transfer among atoms and are performed on parallel computers. During the oxide growth, large pressure variations occur that result in rapid diffusion of atoms in the oxide. The large negative pressure contribution from electrostatic forces in the oxide is partially offset by the positive contribution of steric repulsion. This results in the oxide remaining largely under negative pressure, which causes aluminum to diffuse toward the surface and oxygen to diffuse toward the interior of the cluster. The diffusivity of aluminum is 30% to 60% higher than that of oxygen in the oxide. Structural analysis reveals that a 40 Å thick amorphous oxide scale consisting of mixed octahedral, $\text{Al}(\text{O}_{1/6})_6$, and tetrahedral, $\text{Al}(\text{O}_{1/4})_4$, configurations is formed during 466 ps of simulation time. This is in excellent agreement with experimental results on aluminum nanoclusters. The average mass density in the oxide scale is 75% of the crystalline alumina density. Owing to variations in aluminum and oxygen densities, structures in the oxide scale vary when passing through the oxide from the metal-oxide interface to the oxide-environment interface. Currently we are investigating

the behavior of nanostructured composites, consisting of passivated aluminum nanoclusters (these simulations involve 100 nanoclusters obtained from the canonical simulation, each consisting of 400 000 atoms).

We are deeply indebted to Dr. Michael Berman for suggesting this problem. This work was supported by NSF, U.S. DOE, AFOSR, Army Research Office, USC-LSU Multidisciplinary University Research Initiative, Petroleum Research Fund, NSF-JSPS USA-Japan International grant, and Louisiana Education Quality Support Fund. Simulations were performed using the 40-node DEC 4/175 cluster and the 10-node 5/500 cluster systems in the Concurrent Computing Laboratory for Materials Simulations at Louisiana State University, and the 128 processor SGI Origin 2000 system at the Naval Oceanographic Office MSRC.

- [1] H. Gleiter, *Nanostruct. Mater.* **1**, 1 (1992); R. W. Siegel, *Mater. Sci. Eng. A* **168**, 189 (1993).
- [2] R. W. Siegel, *J. Phys. Chem. Solids* **55**, 1097 (1994); E. A. Stern *et al.*, *Phys. Rev. Lett.* **75**, 3874 (1995); R. K. Kalia *et al.*, *Phys. Rev. Lett.* **78**, 689 (1997); R. K. Kalia *et al.*, *ibid.* **78**, 2144 (1997).
- [3] J. C. Sánchez-López *et al.*, *Nanostruct. Mater.* **7**, 813 (1996).
- [4] B. H. Suits *et al.*, *Nanostruct. Mater.* **6**, 609 (1995); T. G. Nieh *et al.*, *Acta Mater.* **44**, 3781 (1996); C. E. Aumann *et al.*, *J. Vac. Sci. Technol. B* **13**, 1178 (1995); J. C. Sánchez-López *et al.*, *J. Mater. Res.* **13**, 703 (1998).
- [5] F. H. Streitz and J. W. Mintmire, *Phys. Rev. B* **50**, 11 996 (1994).
- [6] L. Greengard and V. Rokhlin, *J. Comput. Phys.* **73**, 325 (1987).
- [7] M. Tuckerman *et al.*, *J. Chem. Phys.* **97**, 1990 (1992).
- [8] G. J. Martyna *et al.*, *Mol. Phys.* **87**, 1117 (1996).
- [9] S. Sako *et al.*, *J. Phys. Soc. Jpn.* **59**, 662 (1990).
- [10] S. Ansell *et al.*, *Phys. Rev. Lett.* **78**, 464 (1997).
- [11] I. Levin and D. Brandon, *J. Am. Ceram. Soc.* **81**, 1995 (1998).
- [12] A. J. Bourdillon *et al.*, *Philos. Mag. A* **49**, 341 (1984); S. M. El-Mashri *et al.*, *ibid.* **48**, 665 (1983).
- [13] The explosive nature of aluminum under high oxygen pressure and closed conditions has been observed at NASA Lewis [Ali Sayir (private communication)].